Journal of Alloys and Compounds 773 (2019) 305–313

Contents lists available at ScienceDirect

Journal of Alloys and Compounds

journal homepage: http://www.elsevier.com/locate/jalcom

Mechanical and opto-electrical response of embedded smart composite coating produced via electrodeposition technique for embedded system in defence application

O.S.I. Fayomi [a, b, *], A.A. Atayero [c], M.P. Mubiayi [d], I.G. Akande [e], P.A. Adewuyi [f], M.A. Fajobi [a], W.A. Ayara [g], A.P.I. Popoola [b]

[a] Department of Mechanical Engineering, Covenant University, P.M.B. 1023, Ota, Nigeria
[b] Department of Chemical, Metallurgical and Materials Engineering, Tshwane University of Technology, Pretoria, South Africa
[c] Department of Electrical & Information Engineering, Covenant University, P.M.B. 1023, Ota, Nigeria
[d] Department of Mechanical Engineering, University of Johannesburg, South Africa
[e] Department of Mechanical Engineering, University of Ibadan, Ibadan, Oyo State, Nigeria
[f] Department of Mechatronics Engineering, Bells University of Technology, Ota, Ogun State, Nigeria
[g] Department of Physics, Covenant University, P.M.B. 1023, Ota, Nigeria

ARTICLE INFO

Article history:
Received 31 August 2018
Received in revised form
12 September 2018
Accepted 16 September 2018
Available online 19 September 2018

Keywords:
Microhardness
Coating
Mild steel
Semiconductor
Agglomeration
Optoelectronics

ABSTRACT

The emergence of nanocomposite particulate with the increasing demand for opto-electrical properties for defence application has necessitated this study. In this work, an attempt was made to develop Zn-CeO_2/Zn-CeO_2-Al_2SiO_5 thin film composite on A356 mild steel using electrodeposition technique. The developed coating was attained in 2 V for 10 min at a constant current density of 1.5 A/cm^2 and pH of 4.5. The mass concentration of Al_2SiO_5 was varied, ranging from 0 to 15 g. The composite coatings were characterized using Scanning electron microscope equipped with energy dispersive spectrometer (SEM/EDS). The corroding properties of the coated and uncoated sample were examined through potentiodynamic polarization technique via Autolab PGSTAT 101 Metrohm potentiostat/galvanostat with NOVA software of version 2.1.2 in 3.65% NaCl. The electrical characterization was carried out using voltage-ammeter meter and Keithley 2400 series source meter application tester. The opto-electrical investigation was done using a solar simulator with maximum intensity of 1000 W/m^2 under an air mass of 1.5 at a working intensity of 750 W/m^2. The outcome of various test and characterizations revealed that the electrodeposited Zn-CeO_2/Zn-CeO_2-Al_2SiO_5 possessed good stability, improved microstructural qualities, better electrical conductivity and outstanding corrosion resistance.

1. Introduction

Nano structured metal oxide films have attracted numerous attention in recent years because of their unmatched optical and electronic properties [1]. They are able to form thin-film barrier layers [2,3], strong adhesion, and high stability against mechanical abrasion, high temperatures, and chemical attack [4]. Among the semiconductor nanoparticles, cerium oxide has been of great interest in versatile applications due to its chemical stability and close lattice parameter with silicon which are used in defence electrical system [5,6]. The optical properties of CeO_2 and Al_2SiO_5 films are mainly attributed to the electronic transitions in the UV–visible range, That is to say, addition of CeO_2 and Al_2SiO_5 enhances the ferroelectrics and piezoelectric of steel [7,8]. Semiconductor nanoparticles composite coatings have been observed to improved physicochemical and structural properties. This is why they are frequently used for corrosion control [9]. Although protective surface coatings provide continuous barrier to substrate materials, however, any imperfection along its surface would invariably serve as the focal point for degradation and corrosion of the substrate metal if not quickly controlled [10,11].

Zinc coatings can be considered as one of the main coating methods used for the protection of steel as they have been found to

* Corresponding author. Department of Mechanical Engineering, Covenant University, P.M.B. 1023, Ota, Nigeria.
E-mail addresses: ojo.fayomi@covenantuniversity.edu.ng, Ojosundayfayomi3@gmail.com (O.S.I. Fayomi).

https://doi.org/10.1016/j.jallcom.2018.09.191
0925-8388/

be very cheap, yet extremely effective in improvement of the electrochemical and structural properties of mild steel [12]. Their usage in various industrial sectors as protective coating for large quantities of metal products and other fabricated ferrous metallic parts are enormous [13]. The service life of zinc coating can be enhanced by addition of inert materials into its coating during bath preparation [14]. This inclusion promotes advantageous characteristics for special applications such as semi-conductor, embedded system, defence and optoelectronic components [15,16]. This present research looked into the performance of mild steel coated Zn-CeO_2/Zn-CeO_2-Al_2SiO_5 not only in corrosive environment but also for opto-electrical application.

2. Experimental procedure

2.1. Preparation of substrate

The base metal employed in this research is a rectangular A 356 series mild steel plate whose composition is shown in Table 1. Mild steel of dimension (50 mm × 30 mm x 2 mm) and zinc sheets of (90 mm × 50 mm × 10 mm) were prepared. The cathode was mild steel coupons and anode was the commercially available pure zinc (99.99%). Mild steel was polished with different grades of emery papers.

2.2. Bath formulation

The prepared bath composition with optimised mass concentration is shown in Table 2. The essence of this was to create novel composite plating on mild steel using composite particulates of zinc (Zn), aluminium silicate (Al_2SiO_5), cerium (iv) oxide (CeO_2) in varying proportions with the aim of determining the most effective coating. The bath constituents were varied and applied upon each mild steel plate to examine and obtain the required parameters.

2.3. Deposition of Zn-CeO_2/Zn-CeO_2-Al_2SiO_5

The mild steel substrate prepared earlier was activated by dipping into 10% HCl solution for about 5 s, thereafter rinsed in deionized water. Chemicals of analar grade and deionized water were used in preparing the coating solution at ordinary (room) temperature before coating. The bath formulation was prepared for the coating process and subjected to continuous stirring at 400 rpm and 50 °C constant heating throughout the coating process, to obtain suspension stability and preventing particles' agglomeration. Prevention of agglomeration of particles enhances the mobility electrophoresis of the solution [18]. In the plating process, the degreased mild steel being the cathode was positioned in between two zinc plates and connected to the negative terminal of the rectifier in the electrodeposition bath as shown in Fig. 1. The zinc (anodes) were also immersed and connected to the positive terminal of the rectifier [19,20]. The PH used was 4.5, other plating parameters such as current density, voltage and time were kept at 1.5 A/cm^2, 2.0 V and 10 min respectively as indicated in Table 3. The coatings of the samples were carried out in accordance to ASTM A53/A53M and A153.

Table 1
Chemical Composition of Mild steel sample (%wt).

Elements	C	Mn	Si	P	Al	S	Ni	Fe
Wt %	0.15	0.45	0.18	0.01	0.005	0.031	0.008	Balance

Table 2
Bath concentration and formulation.

Composition	Mass concentration
Zinc Chloride	70 g/L
Cerium (iv) oxide	10 g/L
Boric Acid	5
Glycerin	5 g/L
Aluminum silicate	0–15 g
pH	4.5
Temp.	50 °C
Time	10 min
Current Intensity	1.5 A/cm^2
Thiourea	5 g/L
Sodium Sulphate	5 g/L
Potassium Sulphate	5 g/L

2.4. Characterization of coated samples and structural test

The surface adhesion and chemical reaction of Zn-CeO_2/Zn-CeO_2-Al_2SiO_5 on the mild steel resulted in the development of different phases. The Microstructural evaluations of the phases were carried out by Energy Dispersive Spectroscopy (EDS) and Scanning Electron Microscope (SEM). Keithley 2400 series source meter application tester, Potentiodynamic polarization assessment and Brinell technique were used to characterize the electrical, corrosion and mechanical properties of the coated and uncoated steels.

2.5. Corrosion test

Autolab PGSTAT 101 Metrohm potentiostat/galvanostat equipped with NOVA software of version 2.1.2 was used for the corrosion test. Linear polarization measurement technique was used to determine the corrosion vulnerability of the developed Zn-CeO_2/Zn-CeO_2-Al_2SiO_5 coated steel in 36.5% NaCl by running a Linear Sweep Voltammetry (LSV) and corrosion rate analysis at ambient temperature of 25 °C. The potential was scanned from −1.50–1.50 V versus Ag/AgCl at a scan rate of 0.005 V/s and a step voltage of 0.00045 V, which allows for quasi-stationary state measurements. In view of this, significant corrosion resistance of the composite coated alloys were observed and compared to the uncoated metal. The superior property of Ce composite on Zn-rich electrolyte could be attested to support the structural improvement in corrosion resistance. The adherent precipitating ability of Al^{2+} on the surface of the steel by forming oxide layer is an important factor considered in the choice of Al_2SiO_5 [21–23].

2.6. Electrical properties testing

In order to determine the electrical properties of the coating, the electroplated Mild steel samples were connected in a circuit with a voltmeter and ammeter as shown in Fig. 2. This permits the measurement of resistance and current when Voltage was passed through the samples [24]. Keithley 2400 series source meter application tester and solar simulator were also used for the Electrical properties testing and optical examination respectively. Electrical properties testing were in accordance to ASTM A587 and A606/A606M.

2.7. Microhardness test

The Brinell technique shown in Fig. 3 was used to verify the hardness of coated and uncoated samples. This involves applying a test force (F) through a carbide chunk or hardened steel of diameter (D) during a testing period of 10 s, after which it was removed. The

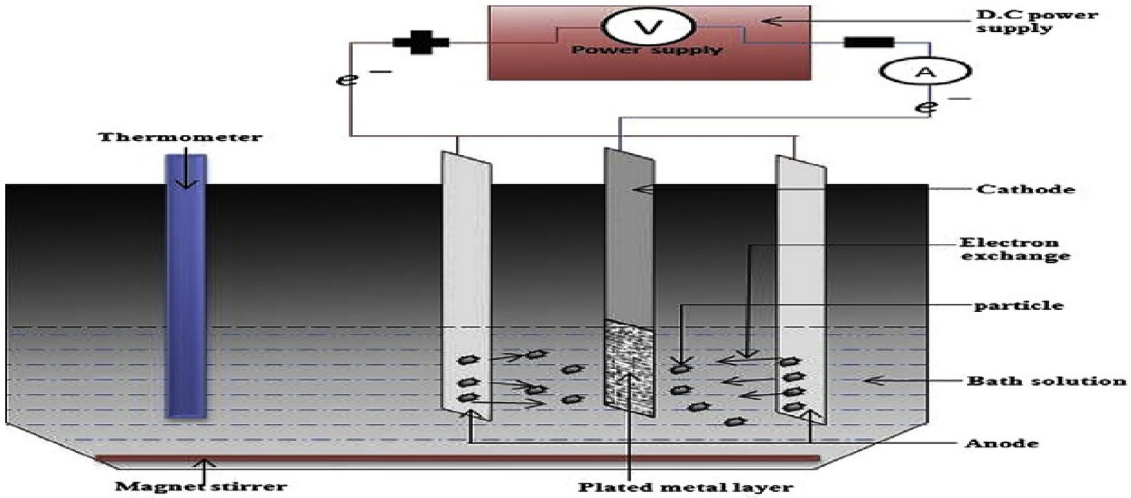

Fig. 1. Schematic diagram of a co-deposition system [17].

Table 3
Electrodeposition parameters of Zn-CeO_2/Zn-CeO_2-Al_2SiO_5 mild steel.

Sample	Time (min)	Voltage	PH	Current Density (A/cm^2)
Zn-10CeO_2	10	2	4.5	1.5
Zn-10CeO_2-5Al_2SiO_5	10	2	4.5	1.5
Zn-10CeO_2-10Al_2SiO_5	10	2	4.5	1.5
Zn-10CeO_2-15Al_2SiO_5	10	2	4.5	1.5

indentation diameters left (D_1) in the test samples were measured using low powered microscope. The indenter covers a distance of 10 mm in order to accommodate most irregularities on surface and sub-surface layer [25,26]. The Brinell hardness numbers can be calculated from equation (1) [27,28].

$$BHN = (2F)\Pi/D\cdot(D - \sqrt{(\text{square of D} - \text{Square of D1})} \quad (1)$$

The hardness test performed was in accordance to ASTM A-370 and A833 [29].

3. Theory/calculation

3.1. Electrical and optical characterization

The essence of electrical characterization is to verify the behaviour of the coated and uncoated steel when current flow through them.

3.1.1. Determination of resistance using ammeter-voltmeter method

This is a simple and quick method of measurement of resistance. It yielded a moderately accurate value over a very wide range of resistances. In this method current through the resistor under test and the potential drop across it was simultaneously measured. The readings were obtained by ammeter and voltmeter respectively. The range of instruments to be used and the voltage required will depend on the size and rating of the resistance under test. A high value resistor will require high-voltage source, a high-range voltmeter and a low-range ammeter, meanwhile a low value resistor will require in most cases a low-voltage, high-current source, a low-range voltmeter and a high-range ammeter.

Current through the ammeter = current through unknown resistance + current through voltmeter

$$I = I_R + I_V$$

$$I_R = I - I_V$$

True value of unknown resistance, $R_x = V/I_R = V/(I - I_V)$

$$Rx = \frac{V}{1(1 - \frac{V}{IRV})} \quad (2)$$

V is the voltmeter reading, R_V is the resistance of voltmeter, and I

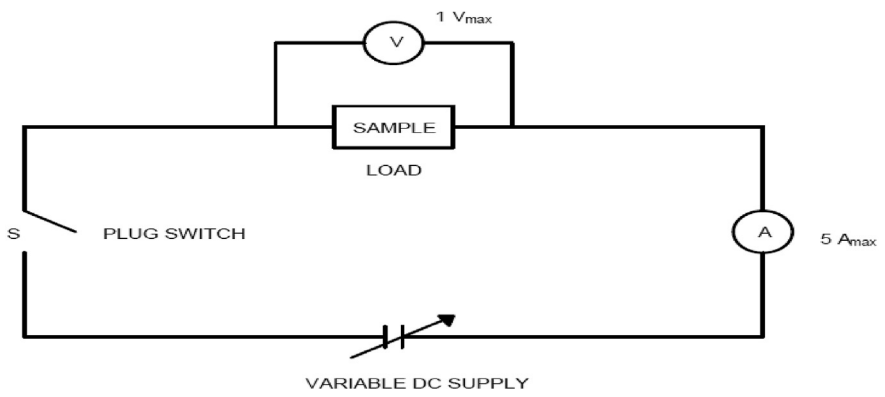

Fig. 2. Electrical testing setup.

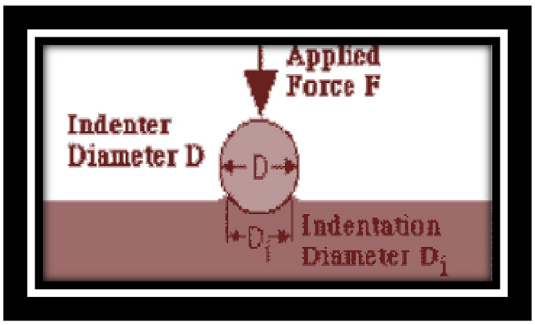

Fig. 3. Schematic illustration of Brinell hardness measurement.

is the current indicated by the ammeter.

The measured value of resistance, $R_m = V/I$.

Substituting $V/I = R_m$ into Eq. (1), we have;

$$Rx = Rm\left(\frac{1}{1-\frac{Rm}{Rv}}\right) \tag{3}$$

From Equation (2), it is clear that the true value of unknown resistance is equal to measured value of unknown resistance provided that voltmeter is of infinite resistance. However, if the voltmeter is of very large resistance as compared to the resistance under measurement.

$R_V \gg R_m$ or R_m/R_V is very small.

Therefore,

$$R_x = R_m\{1 + (R_m/R_V)\} \tag{4}$$

Thus, the measured value of unknown resistance, R_m is lesser than its true value.

Relative error,

$$\varepsilon_r = (R_m - R_x)/R_x \tag{5}$$

3.1.2. Determination of electrical resistivity and conductivity using Keithley 2400 series source meter application tester

A four point probe system attached to Keithley 2400 series source meter with a lab view tracer software interface was also used for the electrical characterization of the coated sample. It was used for the I-V characteristics. It combined wide source with superior ranges of accuracy. The DC current ranges from 1Pa to 1 and DC voltage from 1 μV to 200 V, direct resistance measurement ranges from 1 μΩ to 200 MΩ. With

$$\rho = 2\pi s\left(\frac{V}{I}\right)\Omega cm \text{ for } t \gg s \tag{6}$$

and

$$\rho = \left(\frac{\pi t}{\ln 2}\right)\left(\frac{V}{I}\right)\Omega cm \text{ for } s \gg t \tag{7}$$

t, thickness of the thin film of coat.

For shallow layers, equation (6) gives the sheet resistance as

$$Rs = \frac{\rho}{t} = \frac{\frac{\pi t}{\ln 2}V}{1} = 4.532\left(\frac{V}{I}\right)\Omega cm \text{ for } s \gg t \tag{8}$$

The electrical resistivity is given as

$$\rho = RsXt \tag{9}$$

Rs, sheet resistance, t, film thickness.and the electrical conductivity is given by

$$\varphi = \frac{1}{\rho} \tag{10}$$

It can be seen in equation (8) that by multiplying the recorded measured resistance by 4.532, the result is the sheet resistance, in Ω/square of the film under measurement [30].

The coated sheet electrical resistance, electrical resistivity and electrical conductivity were determined from equations (8)–(10) respectively.

The optical characterization was done using solar simulator. The solar simulator provides a controllable indoor test facility under laboratory conditions. The solar simulator used for this experiment has maximum intensity of 1000 W/m^2 but the experiment was carried out at working intensity of 750 W/m^2. The air mass was 1.5 (same as that of real atmosphere) [30].

4. Results and discussion

4.1. SEM/EDS of deposited composite coating

Figs. 4–7 display the SEM/EDS structure of Zn-10CeO_2, Zn-10CeO_2-5Al_2SiO_5, Zn-10CeO_2-10Al_2SiO_5 and Zn-10CeO_2-15Al_2SiO_5 nano-composites matrices deposited respectively at 1.5 A (current density of 1000 A/m^2) on mild steel. Taking a close look at the four figures, it is visible that the crystallites of the electrocodeposites are homogenously distributed on the substrates. Composite coating often posses better mechanical and corrosion resistance properties when the particles are evenly distributed [30]. The figures further showed the spot analysis of SEM/EDS Spectrum showing CeO_2-riched and Al_2SiO_5-riched portions. It can be observed on the SEM/EDS that the composite thoroughly dispersed on the surface of the substrate, covering it completely. It is worth of note that the nanocomposite structure along the boundary in Fig. 4 is as a result of the integration of visible crystallite of CeO_2 nanoparticulates. Moreover, there are two typical phases in Figs. 5–7, the integration of CeO_2 and Al_2SiO_5 in the zinc interface clearly displayed better nodular structures on the coating network. This was found to increase with the increase in the mass concentration of Al_2SiO_5, which is visible in Fig. 7. Due to the synergistic and complementary effect of CeO_2 and Al_2SiO_5 nano particles incorporated to strengthen the coating system, the coating surface and the interface of Zn-CeO_2/Zn-CeO_2-Al_2SiO_5 coated have been given a refined morphology making it look attractive. This was actually expected since the path of nucleation started from the zinc metal as load carrier; the dissemination of the particulates involves the nucleation domains and therefore improving the formed nanocomposites [31–33].

Furthermore, it is significant to indicate that the slight change in microstructure among Figs. 5–7 might be traceable to the increase in the mass concentration of Al_2SiO_5 nanoparticulates integrated in the nanocomposite coatings resulting to enriched precipitation and enhanced reinforcement. Also, with reference to [34], the induced current density along with other coating constraints together with the quantity of coating particulates can also play vital role in modification of the coating and surface quality of an electrocodeposites material. It is obvious from the EDS in Fig. 4 that the dispersive strengthening and grain filling effects of CeO_2 in Zn-CeO_2 coated steel have become stronger in Figs. 5–7 with the increase in Al_2SiO_5 particles. One can therefore conclude that the hardness of

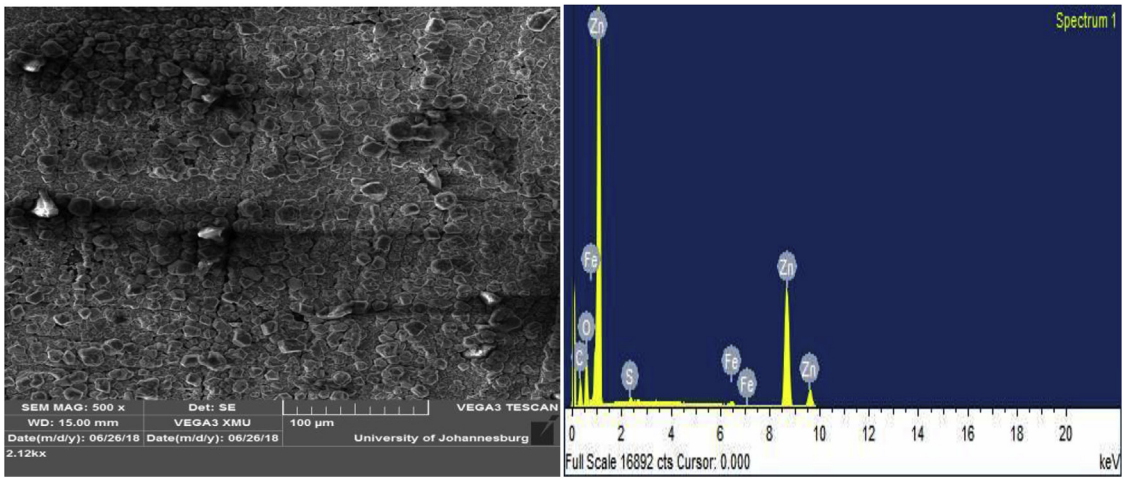

Fig. 4. SEM/EDS structure of Zn-10CeO_2 coated steel.

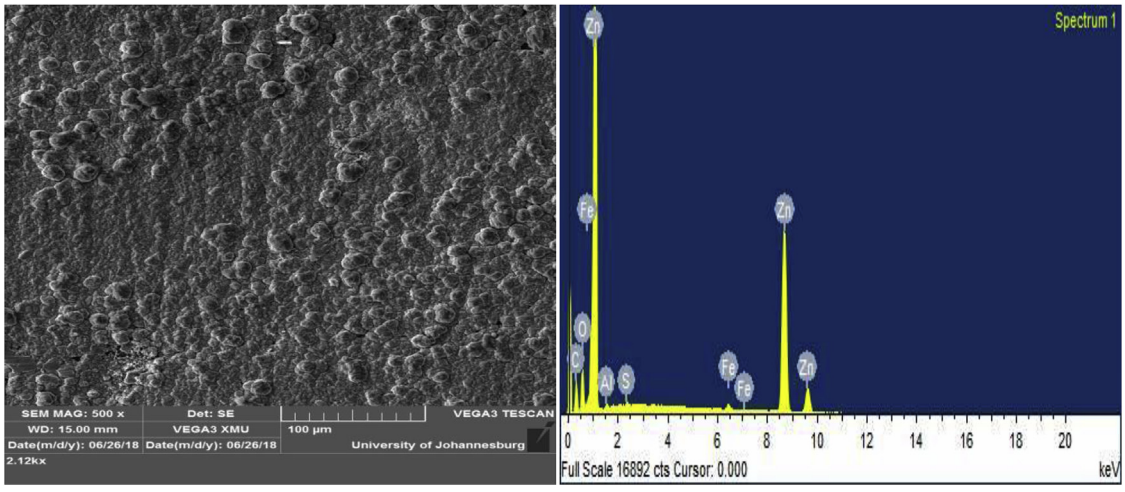

Fig. 5. SEM/EDS structure of Zn-10CeO_2- Al_2SiO_5 coated steel.

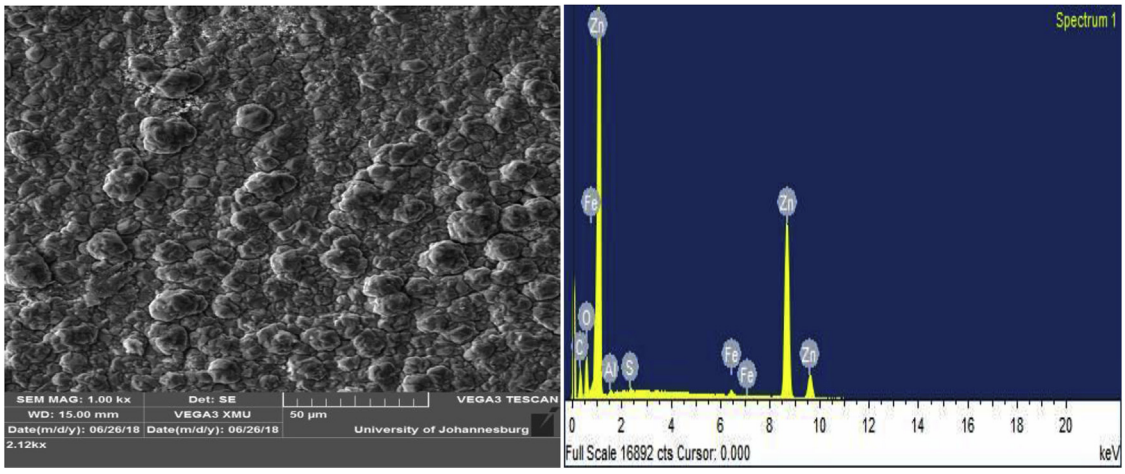

Fig. 6. SEM/EDS structure of Zn-10CeO_2- Al_2SiO_5 coated steel.

the composite coatings increased with the incorporation of Al_2SiO_5 particles in the coating. This is in accordance to the finding of other authors [35,36].

4.2. Electrochemical test result

The values of corrosion current density (Icorr), corrosion

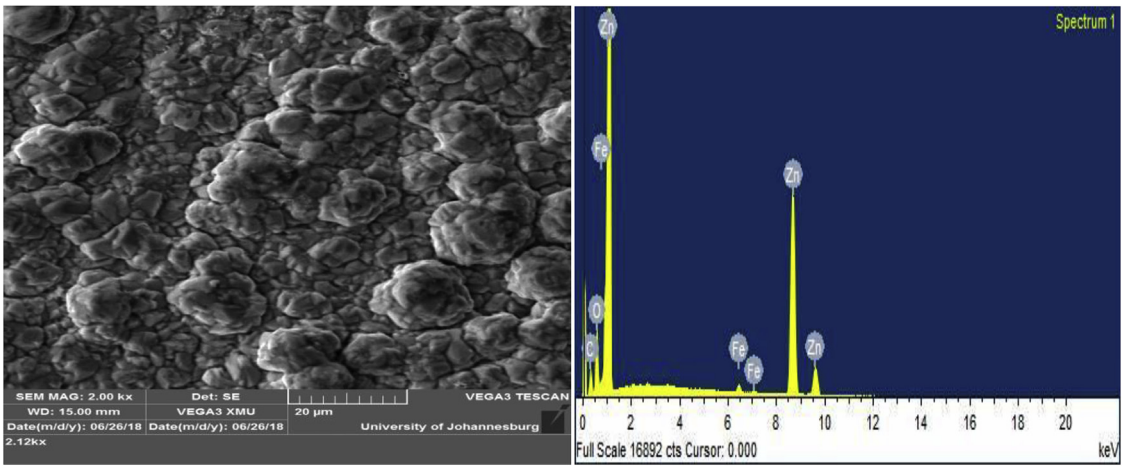

Fig. 7. SEM/EDS structure of Zn-10CeO_2-15Al_2SiO_5 coated steel.

potential (Ecorr), corrosion rate (CR) and polarization potential (R_P) of the coated and uncoated samples in 3.65% NaCl were obtained from the extrapolation of Tafel plot shown in Fig. 8. The results reveal the corrosion resisting characteristics of the particles in the test solution. The values of corrosion current density of the coated samples were found to be smaller than that of the uncoated. This shows that the coating blocked the active sites of the steel preventing exchange of current. The coatings were able to form inhibition barriers, therefore preventing the cathodic evolution and anodic metal dissolution reactions of the mild steel [37,38]. Zn-CeO_2/Zn-CeO_2-Al_2SiO_5 composite coatings are mixed inhibitors but less negative values of the Ecorr of the coated samples with respect to the control signify that the coatings acted predominantly as anodic inhibitors. Corrosion rate of Zn-10CeO_2-5Al_2SiO_5 coated sample was the least with the corrosion rate of 0.0171 (mm/yr) as indicated in Table 4. This may be traceable to the nature and tenacity of the passive film produced by Zn-10CeO_2-5Al_2SiO_5 on the surface of the coated steel or chemical stability of the samples [39]. Hence, it worthy of note that the effect of Zn-CeO_2/Zn-CeO_2-Al_2SiO_5 coated steel at 1.5 A exhibited optimal corrosion resistance in salt solution. These results were in good agreement with the results obtained by other authors, ref. [40–42].

4.3. Microhardness behaviour of Zn-CeO_2/Zn-CeO_2-Al_2SiO_5 deposition

The microhardness results obtained for the Zn-CeO_2/Zn-CeO_2-Al_2SiO deposit is displayed in Fig. 9. Upon comparison Zn-10CeO_2-10Al_2SiO gave the highest hardness reading. Using the brinell hardness value the substrate material hardness increased from 177 BHN to 203 BHN for the electrodeposited sample. This is in accordance to ASTM A-370 and A833. In general, the hardness value for all the samples with varying additives shows an increase. This further implies that the improvement in hardness can be attributed to the formation of adhesive mechanism of the composite coating on the substrate sample. Also, micro hardness of electrodeposited coatings is dependent on operating factors such as bath constituents and other processing parameters [43].

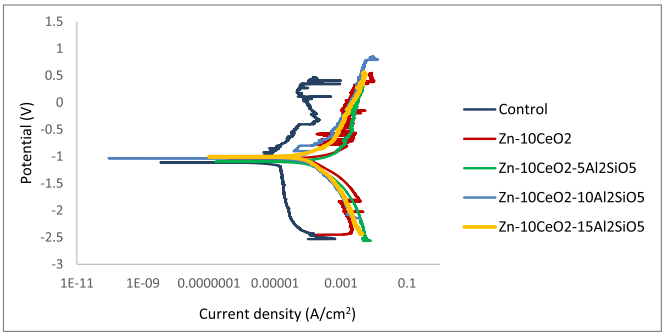

Fig. 8. Potentiodynamic Polarization Curves of Zn-CeO_2/Zn-CeO_2-Al_2SiO_5 coated and uncoated samples.

4.4. Weight loss results of Zn-CeO_2/Zn-CeO_2-Al_2SiO_5 deposition

For the Weight loss experiment carried out in accordance to ASTM A90/A90M, the uncoated and coated samples immersed in 36.5% NaCl and allowed to corrode for 30 days under uniform conditions. Investigations and measurements were made at 5 days interval. The result of the observation is displayed in Fig. 10. The loss in mass of the uncoated samples was found to be higher than the coated samples. It was observed that Zn-10CeO_2-15 Al SiO_5 coated mild steel has the least mass lost rate which can be attributed to the formation oxide layer over the surface of the steel as a result of larger mass concentration of Aluminium in the composite.

4.5. Coating thickness of Zn-CeO_2/Zn-CeO_2-Al_2SiO_5 deposition

Coating thickness is an important parameter for evaluating coating performance in codeposition process. It is used to examine the coating's characteristics, expected life span, strength and to a large extent the uniformity of the deposited layer especially when both faces of an electroplated body are compared. From the coating thickness chart shown in Fig. 11, Zn-10CeO_2-15Al_2SiO_5 coated steel attained the highest value of thickness. This was also confirmed by the SEM/EDS structure in Fig. 7. The reason for this could be as a result of higher concentration of the particulates embedded in the electrolyte. This can also be attributed to due to the adhesive property of the coating and the physical size particles of Al_2SiO_5 particles.

4.6. Electrical characterization result of Zn-CeO_2/Zn-CeO_2-Al_2SiO_5 deposition

The results vary due to the unpredictability and unconformity in the nature of electricity. It was observed from the tests carried out,

Table 4
Potentiodynamic Polarization Data of Zn-CeO_2/Zn-CeO_2-Al_2SiO_5 coated and uncoated samples.

Sample	Icorr (A/cm^2)	RP (Ω)	Ecorr (V)	Corrosion rate (mm/yr)
CONTROL	2.04E-4	198	−1.2122	2.57
Zn-10CeO_2	3.38E-07	3184	−1.0942	0.0254
Zn-10CeO_2-5Al_2SiO_5	1.47E-07	4050	−1.0660	0.0171
Zn-10CeO_2-10Al_2SiO_5	3.853E-06	1890	−1.0969	0.0445
Zn-10CeO_2-15Al_2SiO5	2.19E-06	2197	−1.1086	0.0439

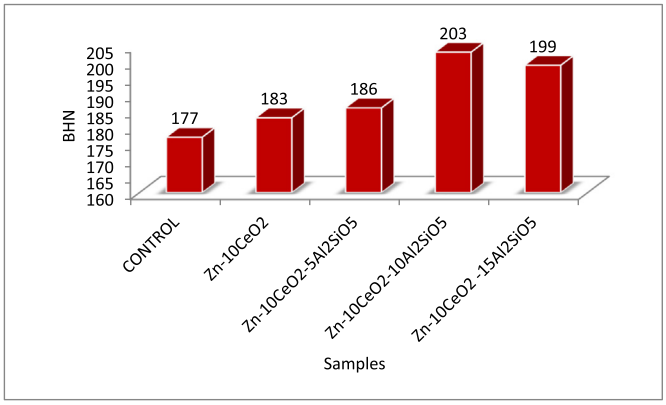

Fig. 9. Brinell hardness value for Zn-CeO_2-Al_2SiO_5 Deposition.

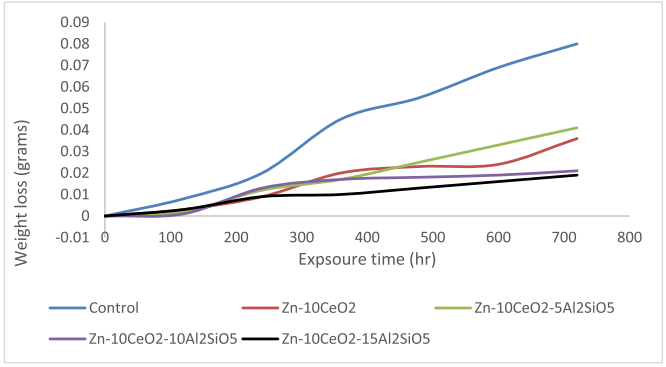

Fig. 10. Weight loss for Zn-CeO_2/Zn-CeO_2-Al_2SiO_5 based matrix.

that the electrodeposition of the co-deposited materials added to the base metal improved electrical properties. Maximum current of 1.8 A was made to pass through the coated and the uncoated samples. It was observed as shown in Fig. 12 and Table 5 that the uncoated steel possesses the least conductance value of 1.0989Ω^{-1} while Zn-10CeO_2-15Al_2SiO_5 coated steel has the highest, 1.6393Ω^{-1}. The coated samples possess higher conductance values indicating that Zn-CeO_2/Zn-CeO_2-Al_2SiO_5 composite have the tendency to increase the conductivity of the steel. This might be attributed to the good electrical properties ion of Ce in the coating. However, reverse is the case for resistivity. The uncoated sample as shown in Fig. 13 displayed the maximum resistivity of 41.81 Ωm. Zn-10CeO_2 was found to exhibit the least resistivity value of 31.93 Ωm.

It can therefore be concluded that the coated samples are better conductor of electricity than the uncoated sample. The reason for this improvement could be attributed to the better stability of photon current by the active nature of Zn-CeO_2/Zn-CeO_2-Al_2SiO_5 coating system. Zn-CeO_2/Zn-CeO_2-Al_2SiO_5 nano-composites coating showed better performance under the light than the dark position. The reason for this are the electrons that were photo generated during illumination [44,45]. It was also observed that the current flow under light decreases more linearly with resistance when compared to the dark situation. This notable effect could be attributed to the photo electron stability of light energy from the solar simulator [44,46].

5. Conclusion

- CeO_2 and Al_2SiO_5 nanoparticulates were used to produce Zn-CeO_2/Zn-CeO_2-Al_2SiO_5 nanocomposite coating from Sulphide bath.
- The integration of the CeO_2/Al_2SiO_5 composite particles in the zinc matrix as reinforcement improved the structural properties and dispersion of grain across the lattice.
- Zn-CeO_2/Zn-CeO_2-Al_2SiO_5 nanocomposite displayed improved conductivity and resistivity of mild steel which could be applied for extended application.
- The electrochemical result showed that Zn-CeO_2/Zn-CeO_2-Al_2SiO_5 nano composite exhibited good corrosion resistance in 3.65% NaCl

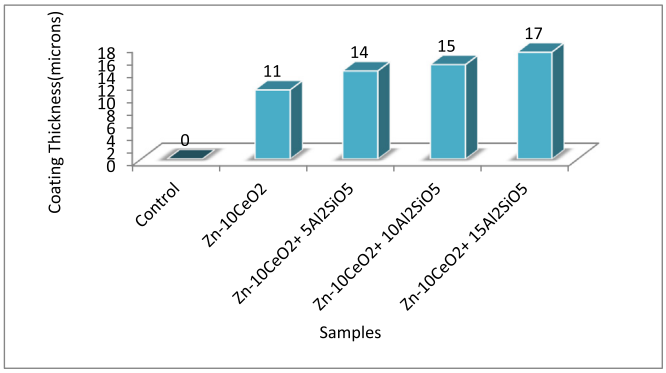

Fig. 11. Coating Thickness of Zn-CeO_2/Zn-CeO_2-Al_2SiO_5 based matrix.

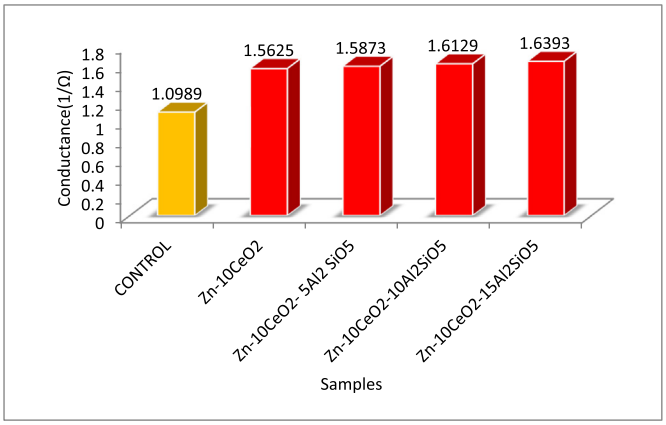

Fig. 12. Maximum Conductance of Zn-CeO_2/Zn-CeO_2-Al_2SiO_5 based matrix.

Table 5
Electrical properties of uncoated and coated samples.

Samples	Coating Thickness t (microns)	Resistivity ρ(Ωm)	Conductivity $\varphi\left(\frac{1}{\Omega m}\right)$	Conductance c (1/Ω)
Control	0	41.81	0.024	1.0989
Zn-10CeO_2	11	31.98	0.031	1.5625
Zn-10CeO_2-5Al_2SiO_5	14	34.54	0.029	1.5873
Zn-10CeO_2-10Al_2SiO_5	15	36.25	0.028	1.6129
Zn-10CeO_2-15Al_2SiO_5	17	38.27	0.026	1.6393

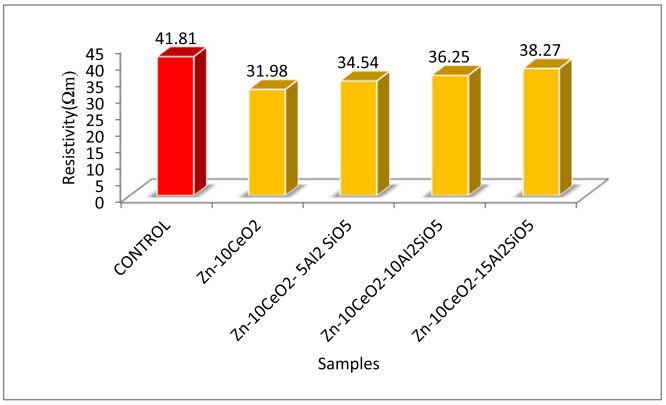

Fig. 13. Resistivity of Zn- Zn-CeO_2/CeO_2-Al_2SiO_5 based matrix.

❖ The study has provided useful knowledge on the film application of nano composite deposition for optoelectrical, corrosion and structural properties.

References

[1] I.R. De Larramendi, N. Ortiz-Vitoriano, B. Acebedo, D.J. De Aberasturi, I.G. De Muro, A. Arango, E. Rodríguez-Castellón, J.I. De Larramendi, T. Rojo, Pr-doped ceria nanoparticles as intermediate temperature ionic conductors, Int. J. Hydrogen Energy 17 (2011) 10981–10990.

[2] T. Inoue, M. Osonoe, H. Tohda, M. Hiramatsu, Y. Yamamoto, A. Yamanaka, T. Nakayama, Low-temperature epitaxial growth of cerium dioxide layers on (111) silicon substrates, J. Appl. Phys. 12 (1991) 813–815.

[3] Y.S. Lee, J. Heo, S.C. Siah, J.P. Mailoa, R.E. Brandt, S.B. Kim, R.G. Gordon, T. Buonassisi, Ultrathin amorphous zinc-tin-oxide buffer layer for enhancing heterojunction interface quality in metal-oxide solar cells, Energy Environ. Sci. 7 (2013) 2112–2118.

[4] R.G. Toro, G. Malandrino, I.L. Fragalà, R. Lo Nigro, M. Losurdo, G. Bruno, Relationship between the nanostructures and the optical properties of CeO_2 thin films, J. Phys. Chem. B 42 (2004) 16357–16364.

[5] N.K. Renuka, Structural characteristics of quantum-size ceria nano particles synthesized via simple ammonia precipitation, J. Alloys Compd. 513 (2012) 230–235.

[6] S. Wang, W. Wang, J. Zuo, Y. Qian, Study of the Raman spectrum of CeO_2 nanometer thin films, Mater. Chem. Phys. 6 (2001) 246–248.

[7] S. Aryal, P. Rulis, W.Y. Ching, Density functional calculations of the electronic structure and optical properties of aluminosilicate polymorphs (Al_2SiO_5), Am. Mineral. 1 (2008) 114–123.

[8] X. Wang, H.L. Chan, C.L. Choy, Piezoelectric and dielectric properties of CeO_2-added (Bi0. 5Na0. 5) 0.94 Ba0. 06TiO_3 lead-free ceramics, Solid State Commun. 8 (2003) 395–399.

[9] O.S. Fayomi, A.P. Popoola, Development of smart oxidation and corrosion resistance of multi-doped complex hybrid coatings on mild steel, J. Alloys Compd. 637 (2015) 382–392.

[10] M.T. Bankole, A.S. Abdulkareem, J.O. Tijani, S.S. Ochigbo, A.S. Afolabi, W.D. Roos, Chemical oxygen demand removal from electroplating wastewater by purified and polymer functionalized carbon nanotubes adsorbents, Water Res. Ind. 18 (2017) 33–50.

[11] D.A. Winkler, M. Breedon, P. White, A.E. Hughes, E.D. Sapper, I. Cole, Using high throughput experimental data and in silicon models to discover alternatives to toxic chromate corrosion inhibitors, Corrosion Sci. 106 (2016) 229–235.

[12] V.S. Aigbodion, O.S. Fayomi, Anti-corrosion coating of mild steel using ternary Zn-ZnO-Y_2O_3 electro-deposition, Surf. Coating. Technol. 306 (2016) 448–454.

[13] H.C. Chuang, G.Y. Hong, J. Sanchez, Fabrication of high aspect ratio copper nanowires using supercritical CO_2 fluids electroplating technique in AAO template, Mater. Sci. Semicond. Process. 5 (2016) 17–26.

[14] O.S. Fayomi, A.P. Popoola, Anti-corrosion and tribo-mechanical properties of Co-deposited Zn–SnO_2 composite coating, Acta Metall. Sin. (Engl. Lett.) 4 (2015) 521–530.

[15] S.A. El-Enin, O.E. Abdel-Salam, H. El-Abd, A.M. Amin, New electroplated aluminum bipolar plate for PEM fuel cell, J. Power Sources 1 (2008) 131–136.

[16] V.S. Aigbodion, O.S. Fayomi, Surface characterization, mechanical properties and corrosion behaviour of ternary based Zn–ZnO–SiO_2composite coating of mild steel, J. Alloys Compd. 654 (2016) 561–566.

[17] O.S. Fayomi, V.S. Aigbodion, Effect of thermal treatment on the interfacial reaction, microstructural and mechanical properties of Zn–Al–SnO_2/TiO_2 functional coating alloys, J. Alloys Compd. 617 (2014) 455–463.

[18] A.A. Daniyan, L.E. Umoru, O.S. Fayomi, Structural Evolution, Optoelectrical and Corrosion Properties of Electrodeposited WO_3 Integration on Zn-tio$_2$ Electrolyte for Defence Super Application, Defence Technology, 2018.

[19] S.S. Achi, Basic Principles of Coating Technology. Shemang Graphics, Zaria Nigeria, 2003, pp. 1–2.

[20] O.S. Fayomi, M. Abdulwahab, Property's evaluation of ternary surfactant-induced Zn-Ni-Al_2O_3 films on mild steel by electrolytic chemical deposition, J. Ovonic Res. 5 (2013) 123–132.

[21] O.S. Fayomi, M. Abdulwahab, A.P. Popoola, F. Asuke, Corrosion resistance of AA6063-Type Al-Mg-Si alloy by silicon carbide in sodium chloride solution for marine application, J. Mar. Sci. Appl. 4 (2015) 459–462.

[22] K. Krishnaveni, J. Ravichandran, Effect of aqueous extract of leaves of Morinda tinctoria on corrosion inhibition of aluminium surface in HCl medium, Trans. Nonferrous Metals Soc. China 8 (2014) 2704–2712.

[23] O.S. Fayomi, M. Abdulwahab, Degradation behaviour of aluminium in 2M HCl/HNO_3 in the presence of arachis hypogeae natural oil, Int. J. Electrochem. Sci. 7 (2012) 5817–5827.

[24] K.F. Ayarkwa, S.W. Williams, J. Ding, Assessing the effect of TIG alternating current time cycle on aluminium wire+ arc additive manufacture, Addit. Manuf. 18 (2017) 186–193.

[25] S. Nagaraja, U.N. Kempaiah, Influence of ceramic particulate reinforcements on fly ash dispersion strengthened composites for aircraft structures, J. Aero. Eng. Technol. 3 (2018) 38–45.

[26] H.R. Ammar, F.M. Haggag, A.S. Alaboody, F.A. Al-Mufadi, Nondestructive measurements of flow properties of nanocrystalline Al-Cu-Ti alloy using automated ball indentation (ABI) technique, Mater. Sci. Eng. A 729 (2018) 477–486.

[27] Y.H. Babu, D.B. Rao, Production and characterisation of aluminum–titanium di boride composite using powder metallurgy technique, Int. J. Eng. Manag. Res. (IJEMR) 3 (2017) 312–317.

[28] Ram JK, Singh M. Process Parameters Optimization for Friction Stir Welding of the Hardness of AL 6063 Alloy using Taguchi Technique.

[29] H. Soares, T. Zucarelli, M. Vieira, M. Freitas, L. Reis, Experimental characterization of the mechanical properties of railway wheels manufactured using class B material, Procedia Struct. Integr. 1 (2016 Jan 1) 265–272.

[30] A.A. Daniyan, L.E. Umoru, A.P. Popoola, O.S. Fayomi, Opto-electrical and corrosion properties of electrocodeposites Zn-TiO_2/WO_3-ZnO-SnO_2 nano-composite coatings, Mater. Corros. 6 (2018) 725–735.

[31] T. Oluyori, O.E. Olorunniwo, O.S. Fayomi, P.O. Atanda, Performance evaluation effect of Nb_2O_5 particulate on the microstructural, wear and anti-corrosion resistance of Zn–Nb_2O_5 coatings on mild steel for marine application, J. Bio-Tribo-Corrosion 4 (2017) 51.

[32] K.S. Alhawari, M.Z. Omar, M.J. Ghazali, M.S. Salleh, M.N. Mohammed, Wear properties of A356/Al2O3 metal matrix composites produced by semisolid processing, Procedia Eng. 68 (2013) 186–192.

[33] I. Ahmed, Z. Ahmad, F. Patel, M.S. Khan, A photo-cathodic protection system utilizing UV radiations, Int. J. Eng. Technol. 1 (2011) 197–202.

[34] R. Subasri, T. Shinohara, K. Mori, Modified TiO2 coatings for cathodic protection applications, Sci. Technol. Adv. Mater. 5 (2005) 501.

[35] A. Akarapu, Surface Property Modification of Copper by Nanocomposite Coating, M.Tech. Thesis, Indian: Department of Metallurgical and Materials Engineering, National Institute of Technology, Rourkela, 2011.

[36] K.S. Alhawari, M.Z. Omar, M.J. Ghazali, M.S. Salleh, M.N. Mohammed, Wear properties of A356/Al_2O_3 metal matrix composites produced by semisolid processing, Procedia Eng. 68 (2013) 186–192.

[37] A. Dutta, S.K. Saha, U. Adhikari, P. Banerjee, D. Sukul, Effect of substitution on corrosion inhibition properties of 2-(substituted phenyl) benzimidazole derivatives on mild steel in 1 M HCl solution: a combined experimental and theoretical approach, Corrosion Sci. 123 (2017) 256–266.

[38] L. Rossrucker, A. Samaniego, J.P. Grote, A.M. Mingers, C.A. Laska, N. Birbilis, G.S. Frankel, K.J. Mayrhofer, The pH dependence of magnesium dissolution and hydrogen evolution during anodic polarization, J. Electrochem. Soc. 7 (2015) 333–339.
[39] A.P.I. Popoola, A.A. Daniyan, L.E. Umoru, O.S.I. Fayomi, Effect of WO_3 nanoparticles loading on the microstructural, mechanical and corrosion resistance of Zn matrix/TiO_2-WO_3 nanocomposite coatings for marine application, J. Mar. Sci. Appl. 16 (2017), 1389-7.
[40] B.M. Praveen, T.V. Venkatesha, Electrodeposition and corrosion resistance properties of Zn- Ni/TiO2 nano composite coatings, Int. J. Electrochem. 2011 (2011).
[41] O.S. Fayomi, A.P.I. Popoola, Study of Al2O3/SiC particle loading on the microstructural strengthening characteristics of Zn–Al2O3–SiC matrix composite coating, Egypt. J. Basic Appl. Sci. 2 (2014) 120–125.
[42] R.R. Moreira, T.F. Soares, J. Ribeiro, Electrochemical investigation of corrosion on AISI 316 stainless steel and AISI 1010 carbon steel: study of the behaviour of imidazole and benzimidazole as corrosion inhibitors, Adv. Chem. Eng. Sci. 4 (2014) 503.
[43] D.E. Rusu, A. Ispas, A. Bund, C. Gheorghies, G. Carac, Corrosion tests of nickel coatings prepared from a Watts-type bath, J. Coating Technol. Res. 1 (2012) 87–95.
[44] P.E. Agbo, M.N. Nnabuchi, Core-shell TiO_2/ZnO Thin film: preparation, characterization and effect of Temperature on some selected properties, Chalcogenide Lett. 8 (2011) 4.
[45] J. Fustes, A. Gomes, M.I. da Silva Pereira, Electrodeposition of Zn–TiO_2 nanocomposite films—effect of bath composition, J. Solid State Electrochem. 11 (2008) 1435–1443.
[46] M. Okada, K. Tajima, Y. Yamada, K. Yoshimura, Photocatalytic performance of very thin TiO_2/SnO_2 stacked-film prepared by magnetron sputtering, Vacuum 3 (2008) 688–690.